Signal Enhancement for Magnetic Navigation Challenge Problem

Albert R. Gnadt[1], Joseph Belarge[2], Aaron Canciani[3], Lauren Conger[2], Joseph Curro[3], Alan Edelman[1], Peter Morales[2], Michael F. O'Keeffe[2], Jonathan Taylor[2], and Christopher Rackauckas[1]

[1]Massachusetts Institute of Technology, Cambridge, MA, USA
[2]MIT Lincoln Laboratory, Lexington, MA, USA
[3]Air Force Institute of Technology, Dayton, OH, USA

July 24, 2020

1 Introduction

Harnessing the magnetic field of the earth for navigation has shown promise as a viable alternative to other navigation systems. Commercial and government organizations have surveyed the earth to varying degrees of precision by collecting and storing magnetic field data as magnetic anomaly maps. A magnetic navigation system collects its own magnetic field data using a magnetometer and uses magnetic anomaly maps to determine the current location. This technique does not rely on satellites or other external communications, and it is available globally at all times and in all weather.

The greatest challenge with magnetic navigation arises when the magnetic field data from the magnetometer on the navigation system encompass the magnetic field from not just the earth, but also from the vehicle on which it is mounted. The total magnetic field is a linear superposition of the magnetic fields of the vehicle and the earth (with additional contributions from sources arising from diurnal variation and space weather, which can be largely removed using ground-based reference measurements), and the magnetometer reports the scalar magnitude of the net magnetic field vector. It is difficult to separate the earth magnetic anomaly field magnitude, which is crucial for navigation, from the total magnetic field magnitude reading from the sensor.

Research was sponsored by the United States Air Force Research Laboratory and was accomplished under Cooperative Agreement Number FA8750-19-2-1000. The views and conclusions contained in this document are those of the authors and should not be interpreted as representing the official policies, either expressed or implied, of the United States Air Force or the U.S. Government. The U.S. Government is authorized to reproduce and distribute reprints for Government purposes notwithstanding any copyright notation herein.

The purpose of this challenge problem is to decouple the earth and aircraft magnetic signals in order to derive a clean signal from which to perform magnetic navigation. Baseline testing on the dataset shows that the earth magnetic field can be extracted from the total magnetic field using machine learning (ML). The challenge is to remove the aircraft magnetic field from the total magnetic field using a trained neural network. These challenges offer an opportunity to construct an effective neural network for removing the aircraft magnetic field from the dataset, using an ML algorithm integrated with physics of magnetic navigation.

2 Magnetic Navigation Background

Magnetic navigation is enabled by variations in the crustal magnetic field of the earth, also known as the magnetic anomaly field. The total geomagnetic field is comprised of fields from several sources, the most dominant of which is the core field with values ranging from 25 to 65 microtesla at the surface of the earth, about 100 times weaker than a refrigerator magnet. The magnetic anomaly field typically varies by hundreds of nanotesla, 100 times weaker than the core field. As such, magnetic navigation requires the ability to sense small differences in the crustal magnetic field, which can be mapped and is stable over geologic time spans. The spatial extent of the crustal fields make the fields strong enough for navigation even at tens of kilometers altitude above the earth's surface.

The strength of a static magnetic field arising from a localized source follows the inverse cubic distance scaling law of a magnetic dipole (when the distance to the source is much larger than the spatial extent of the source). This high drop-off rate in magnetic fields means that it is difficult for disturbances to affect magnetic sensors from a distance without exhorting a significant amount of power, making it difficult to interfere with or jam magnetic navigation from ground stations. Thus, the predominant issue with magnetic navigation comes from magnetic interference generated by the aircraft itself. The purpose of this challenge is to effectively remove the magnetic interference of the aircraft from the readings of the on-board magnetometers so that effective magnetic navigation can be performed.

Traditionally the earth and aircraft magnetic fields can be separated using the Tolles-Lawson model [1], as described in Appendix A. This process uses bandpass filtered measurements from an additional magnetometer, as well as crucial assumptions about the static nature of the aircraft magnetic field, such as:

1. The magnetic sources on the aircraft arise from permanent dipole, induced dipole, and eddy current fields.
2. The permanent dipole sources do not change over time.
3. The induced dipoles depend on the orientation of the aircraft with respect to the magnetic field of the earth.
4. The inductance from electrical current paths is zero, so the eddy currents arise from instantaneous changes of the magnetic flux through a surface.
5. The total-field anomaly due to the aircraft field is the projection of the aircraft field onto the earth field.

These assumptions are sufficient when the magnetometer is placed on a 3m boom behind the aircraft (tail stinger), because the magnetic field from the aircraft is weak enough relative to the earth at the sensor. However, this is impractical for operational aircraft. The Tolles-Lawson approximation does not produce data with sufficiently accurate results when the magnetometer is close to the multiple magnetic interference sources of the aircraft, such as in the cockpit.

3 Challenge Problem

The goal is to take magnetometer readings from within the cockpit and remove the aircraft magnetic field to yield a clean magnetic signal. The key issue is identifying the desired truth signal, of which two options are presented. One such truth signal is the tail stinger which, after professional compensation, is sufficiently accurate for magnetic navigation. It has the fewest differing conditions from the cockpit sensors due to its location far aft of the cockpit, control surfaces, and other sources of aircraft magnetic interference. However, tail stinger data is not available on all operational aircraft, and using this signal alone would likely cause a model to transfer poorly to other aircraft. The other option is to treat the magnetic anomaly map of the collection region as the truth signal. Using the path of the aircraft, the magnetic anomaly signal of the earth's crust over this path can be determined and treated as the truth signal.

The first case wherein the tail stinger is treated as the truth signal has several advantages. The primary advantage is that there is no need to potentially account for for minor position differences. Additionally, most conditions, such as weather, that were present during the collection would be identical meaning that additional compensation due to known conditions would likely be unnecessary.

The second case wherein the magnetic anomaly map is used as the truth signal yields a case wherein a reference map that would be used for navigation is the target signal. This approach has a major advantage wherein the actual desired signal is the target. However, the map has issues which could make the problem more difficult. First, the signal at the altitude of data collection must be interpolated from the raw map, which adds an additional step of processing. Additionally, the map may be under-sampled in which case the truth data may not be available in the raw map and would need to be interpolated in order to yield the truth signal.

The process of using both truth signals is extremely similar. Both cases can be treated as having 2 outputs; however, each has a natural output that is more useful for evaluation. When training to the tail stinger it is more useful to do a signal comparison rather than comparing to the predicted path along a map as the signal comparison is attempting to determine whether or not the algorithm is learning the aircraft magnetic field. Contrasting this when training to the anomaly map it is more useful to do a comparison to the route as it is possible that the ideal algorithm for navigation purposes is not generating the most optimally enhanced magnetic signal but is instead generating the most optimally enhanced positioning signal.

4 Judging Criteria

For this challenge problem, an evaluation dataset is withheld from participants. The goal is to learn a mechanism for removing the aircraft magnetic field from the build dataset that will generalize to the evaluation dataset. The quality of the submission will be judged according to the root mean squared error (RMSE) compared to the selected truth signal. Detrending may be used to remove any DC offset prior to RMSE calculation. An alternative award for a method that excels in interpretability and verifiability will also be considered. The challenge problem will commence at the JuliaCon 2020 SciML workshop on July 26, 2020 and will run until August 28, 2020. Judging will take place in early September 2020. All submissions should be sent to crackauc@mit.edu in the form of a Git repository with code that can perform predictions on the evaluation dataset without any modifications to the source code required. It is recommended to include an up to 5 page arXiv compatible manuscript that explains the methodology.

5 Description of the Magnetic Navigation Data

A campaign was conducted to collect magnetic field data. During the data collection, flight patterns were planned such that data could be collected at varying heights above ellipsoid (HAE), where the aircraft is flying at a constant altitude above the earth's assumed perfectly ellipsoidal shape, and over varying drape surfaces, where the aircraft is flying at a constant altitude over actual crustal features, such as mountains and valleys.

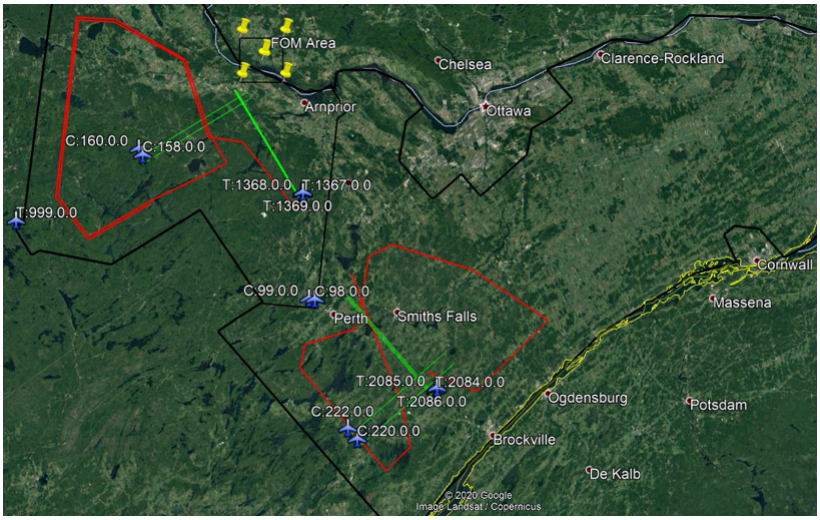

Figure 1: Map showing SGL flight regions. The far west region is the Renfrew flight area. The far east region is the Eastern flight area. The black region labeled FOM is the Figure of Merit area.

The measurements were collected by Sander Geophysics Ltd. (SGL) [2] over Ottawa, Ontario, Canada, using a Cessna Grand Caravan equipped with a number of sensors. The measurements

were collected in three flight areas. The flight area north of Arnprior is the Figure of Merit (FOM) region. The western-most flight area is known as the Renfrew flight area, while the furthest east area is known as the Eastern flight area. All three flight areas are shown in Figure 1.

To collect the total magnetic field measurements, five optically-pumped, cesium split-beam scalar magnetometers, and four vector fluxgate magnetometers were positioned in the aircraft. One scalar magnetometer was positioned on a tail stinger to collect magnetic measurements with minimal aircraft magnetic field noise. The remaining four scalar magnetometers, as well as the three vector magnetometers, were placed inside the cabin of the aircraft. The locations of the sensors within the cabin can be found in Table 1.

Table 1: Summary of Scalar and Vector Magnetometer Locations. The reference point is the front seat rail. X is positive in the aircraft forward direction, Y is positive to port (left facing forward), and Z is positive upward.

Sensor Name	Location	X (m)	Y(m)	Z (m)
	Scalar Magnetometers			
Mag 1	Tail stinger	-12.01	0	1.37
Mag 2	Front cabin aft of cockpit	-0.60	-0.36	0
Mag 3	Mid cabin next to INS	-1.28	-0.36	0
Mag 4	Rear cabin floor	-3.53	0	0
Mag 5	Rear cabin ceiling	-3.79	0	1.20
	Vector Magnetometers			
Flux B	Tail at base of stinger	-8.92	0	0.96
Flux C	Rear cabin port side	-4.06	0.42	0
Flux D	Rear cabin aft side	-4.06	-0.42	0

In addition to the magnetometers, supplemental sensors collected relevant flight data. A subset of this data, such as GPS location, contain information redundant to the truth data. Using this data could lead to falsely accurate neural networks, and therefore should not be used. The data fields shown below were determined to provide information for training, while not providing direct truth data. For information on all data fields collected during flight, see Appendix B.

- DIURNAL
- IGRFMAG1
- UNCOMPMAG2
- UNCOMPMAG3
- UNCOMPMAG4
- UNCOMPMAG5
- FLUXB_X
- FLUXB_Y
- FLUXB_Z
- gradient(FLUXB_X)
- gradient(FLUXB_Y)
- gradient(FLUXB_Z)
- FLUXC_X
- FLUXC_Y
- FLUXC_Z
- gradient(FLUXC_X)
- gradient(FLUXC_Y)
- gradient(FLUXC_Z)
- FLUXD_X
- FLUXD_Y
- FLUXD_Z
- gradient(FLUXD_X)
- gradient(FLUXD_Y)
- gradient(FLUXD_Z)
- INS_ACC_X
- INS_ACC_Y
- INS_ACC_Z
- PITCH
- ROLL
- AZIMUTH
- gradient(PITCH)
- gradient(ROLL)
- gradient(AZIMUTH)
- CUR_COM1
- CUR_ACHi
- CUR_ACLo
- CUR_TANK
- CUR_FLAP
- CUR_STRB
- CUR_SRVO_O
- CUR_SRVO_M
- CUR_SRVO_I
- CUR_IHTR
- CUR_ACPWR
- CUR_OUTPWR
- CUR_BAT1
- CUR_BAT2
- V_ACPWR
- V_OUTPWR
- V_BAT1
- V_BAT2
- V_RESp
- V_RESn
- V_BACKp
- V_BACKn
- V_GYRO1
- V_GYRO2
- V_ACCp
- V_ACCn
- V_BLOCK
- V_BACK
- V_SERVO
- V_CABT
- V_FAN

The truth data for training is an uncorrupted measurement of the magnetic anomaly field. This is provided in two ways: first, in the form of the data collected from the scalar magnetometer located on the tail stinger after professional compensation. This data was collected concurrently among the build dataset, and will provide a direct measurement of the uncorrupted signal. Second, a magnetic anomaly map is provided to determine an alternative truth signal. Magnetic anomaly map data provides a unique measure of the magnetic anomaly field for a location in space, and as such is similar to the magnetic anomaly field data collected from the tail stinger.

Four flights were flown to collect data. Each flight contained a different set of objectives, and as such the dataset from each flight has individual nuances. The details of Flight Number 1003 will be discussed below. For further information on the remaining flights (Flight Numbers 1002, 1004, and 1005) see Appendices C, D, and E.

The objectives for Flight Number 1003 were to measure the crustal magnetic field at two altitudes (400m HAE and 800m HAE) in both the Eastern and Renfrew flight regions. The flight was conducted on June 29, 2020 and lasted approximately five hours and forty-five minutes. A summary of the Line Numbers, which describe when a specific flight segment began and subsequently ended, is shown in Table 2. Line Number 1003.10 has been withheld for the evaluation dataset, while the remaining Line Numbers are provided in the build dataset. Other numbers that do not begin with the Flight Number refer to flight over a survey line.

Table 2: Line Number summary for Flight Number 1003. Line Number 1003.10 has been withheld for the evaluation dataset, while the remaining Line Numbers are provided in the build dataset.

Line Number	Description
1003.01	Takeoff and Transit
1003.02	Eastern Free Fly at 400m HAE
1003.03	Climb to 800m HAE
1003.04	Eastern Free Fly at 800m HAE
1003.05	Transit to Renfrew
1003.06	Descend to 400m HAE
1003.07	Continue transit to Renfrew
1003.08	Renfrew Free Fly at 400m HAE
1003.09	Climb to 800m HAE
1003.10	Renfrew Free Fly at 800m HAE
1003.11	Transit to home

6 Description of the Starter Code

A basic set of starter Julia code files have been provided in the MagNav.jl package within the src folder. This code is largely based on work done by Major Canciani [3]. The files and their function descriptions are described below.

- get_flight_data.jl
  – function get_flight_data: Loads flight data from a saved HDF5 data file and assigns the fields to a struct, which is returned. See get_flight_data.jl file for the full listing of struct fields. To access a field, use dot indexing. Requires the location/name of the file.
  – function readcheck: Only used by function get_flight_data to identify and warn of NaN values in the flight data.

- get_map_data.jl
  – function get_map_data: Loads magnetic anomaly map data from a saved HDF5 data file and assigns the fields to a struct, which is returned. See file for struct fields. To access a field, use dot indexing. Requires the location/name of the file.

- create_TL_Amat.jl
  – function create_TL_Amat: Creates the 18-term Tolles-Lawson "A" matrix discussed in section A.2, which is returned. Requires 3 corresponding magnetic flux measurement vectors.
  – function central_fdm: Central finite difference method for gradient calculation. Requires a vector of values, and returns a same-size vector of gradients.

- create_TL_coef.jl
  – function create_TL_coef: Determines the 18 Tolles-Lawson coefficient vector, which is returned. Requires 3 corresponding magnetic flux measurement vectors (calls function create_TL_Amat) and a scalar magnetic measurement vector from a calibration flight. Optionally accepts a dict of bandpass filter coefficients (pass1, pass2, fs).

- delta_lat_lon.jl
  – function delta_lat: Converts north-south position error (m) to latitude error (rad), which is returned. Requires north-south position error (m) and latitude (rad).
  – function delta_lon: Converts east-west position error (m) to longitude error (rad), which is returned. Requires position error position error (m) and latitude (rad).
  – function delta_north: Converts latitude error (rad) to north-south position error (m), which is returned. Requires latitude error (rad) and latitude (rad).
  – function delta_east: Converts longitude error (rad) to east-west position error (m), which is returned. Requires longitude error (rad) and latitude (rad).

- fft_maps.jl
  – function upward_fft: Upward continuation function for shifting a magnetic anomaly map, which is returned. Requires a magnetic anomaly map matrix (nT), map spacing in each direction (m), and vertical distance for shifting the map (map).
  – function create_K: Only used by function upward_fft.

- gen_interp_map.jl
  – function gen_interp_map: Generates a magnetic anomaly map interpolation, which is re-

turned. Requires a matrix of magnetic anomaly map values (nT), longitude vector (deg), and latitude vector (deg).

- helpers.jl
  – function detrend: Linear regression to remove a trend line (mean, slope) from a vector.
  – function map_grad: Determines the magnetic anomaly map gradient (nT/rad) at a specified position, which is returned (length 2 vector). Requires a magnetic anomaly map interpolation, longitude (deg), and latitude (deg).

A sample run file has also been provided in the MagNav.jl package within the runs folder. Here the usage of each of these functions is shown, and Figure 2 should be plotted as a baseline result. Here, the scalar magnetometers have been compensated using the Tolles-Lawson model, then detrended to remove DC offsets. As shown in Figure 2, the magnetometer 1 (tail stinger) compensation matches the professional compensation done by SGL ("truth" here). Magnetometer 5, despite being located in the cockpit, also performs fairly well, while magnetometers 3 and 4 would not be suitable for magnetic navigation. Magnetometer 2 is not shown due to even worse performance.

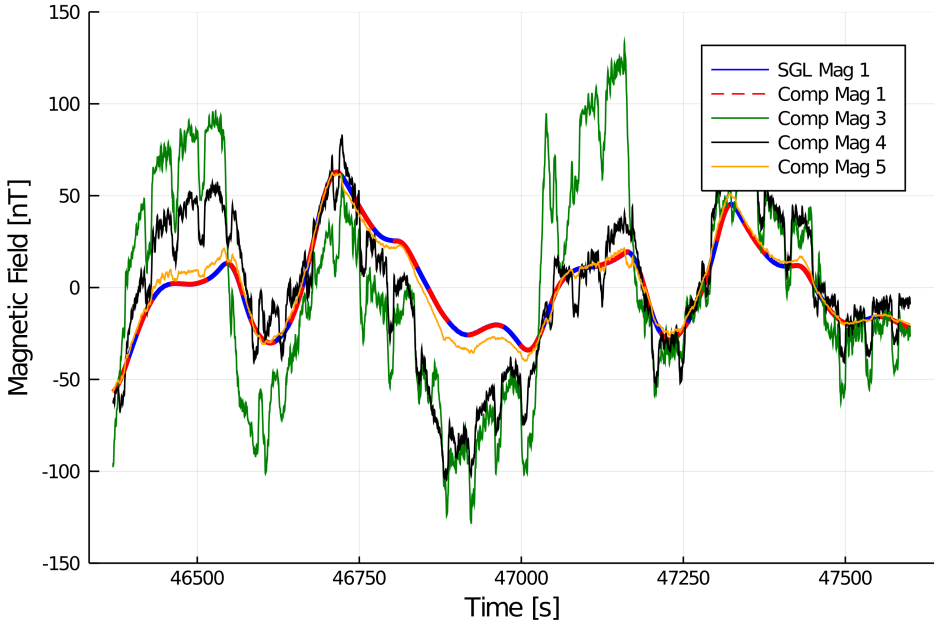

Figure 2: Flight Number 1002 magnetometers compensated using the Tolles-Lawson model.

Appendix A The Tolles-Lawson Model

The Tolles-Lawson model [1] provides a means of isolating the aircraft magnetic field so that it can be removed from the total magnetic field, ideally yielding only the earth magnetic anomaly field used for navigation. The model is derived from a physical model of permanent, induced, and eddy current aircraft magnetic fields, which is presented here. Determining the coefficients of the model hinges on collecting magnetometer data during a calibration flight involving a set of maneuvers performed at a high altitude over a region with a small magnetic gradient (See Figure 3). A bandpass filter removes (ideally) nearly all of the earth magnetic field from the measurements.

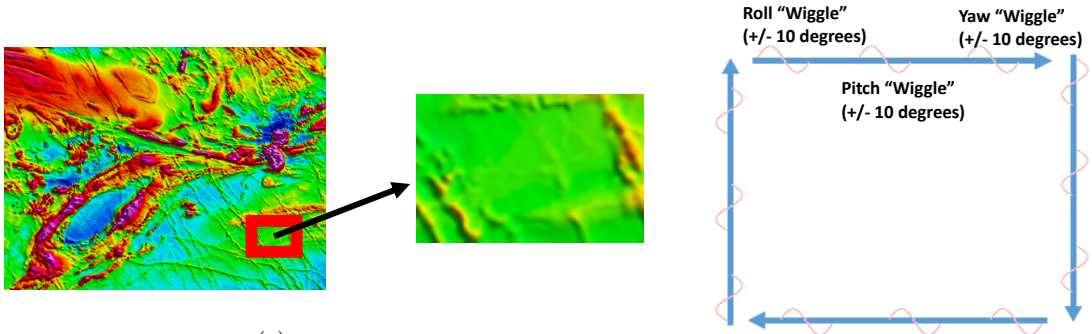

(a) (b)

Figure 3: (a) Magnetic anomaly map with region in red square enlarged to show low magnetic gradients, suitable for a calibration flight. (b) Typical box-like calibration pattern with roll, pitch, and yaw maneuvers conducted along each leg.

A.1 Aircraft Magnetic Fields

Tolles-Lawson uses measurements from a vector magnetometer to remove aircraft magnetic field contributions to the scalar magnetometer measurements, which are used for navigation. It is anticipated that the magnetic dynamics of an operational aircraft will exceed this model, but its assumptions are valid for compensation of the the stinger magnetometer. The Tolles-Lawson procedure considers the projection of the aircraft magnetic field onto the earth magnetic field, whereas a slightly modified version in [4] considers the projection of the aircraft magnetic field onto the total field, which follows here (see Figure 4a).

The total magnetic field vector $\mathbf{H}_t = \mathbf{H}_e + \mathbf{H}_a$ is comprised of the earth $\mathbf{H}_e$ and aircraft $\mathbf{H}_a$ fields (Figure 4a). The reference frame is defined with respect to the transverse, longitudinal, and vertical axes of the aircraft, as shown in Figure 4b. The aircraft magnetic field includes contributions from the permanent magnetic moment, induced magnetic moment, and eddy currents of the aircraft. Their contributions to the magnitude of the total field can be written as

$$H_{at} = \mathbf{P}\mathbf{u}_t + \mathbf{u}_t^T A \mathbf{u}_t + (\mathbf{u}_t^T)' \mathbf{B} \mathbf{u}_t \tag{1}$$

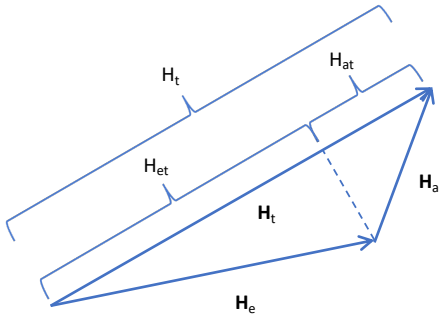

(a)

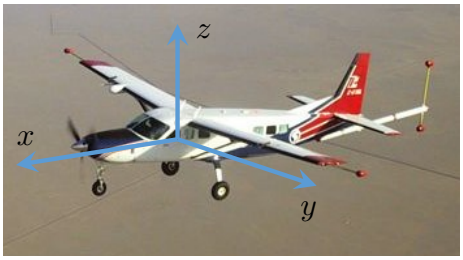

(b)

Figure 4: (a) Earth, aircraft, and total magnetic field vectors with projections of the aircraft and earth magnetic fields onto the total magnetic field. (b) Aircraft coordinate system centered on the front seat rail, where x is positive in the aircraft forward direction, y is positive to port (left facing forward), and z is positive upward.

where the unit vector

$$\mathbf{u}_t = \frac{\mathbf{H}_t}{H_t} = \begin{pmatrix} \cos X \\ \cos Y \\ \cos Z \end{pmatrix} \tag{2}$$

is directly measured by the vector magnetometer, and consists of direction cosines defined by angles X, Y, Z between the total field vector and the respective axes of the reference frame. The coefficient matrices for the permanent moment

$$\mathbf{P} = \begin{pmatrix} p_1 & p_2 & p_3 \end{pmatrix} \tag{3}$$

induced moment

$$\mathbf{A} = \begin{pmatrix} a_{11} & a_{12} & a_{13} \\ a_{21} & a_{22} & a_{23} \\ a_{31} & a_{32} & a_{33} \end{pmatrix} \tag{4}$$

and eddy current

$$\mathbf{B} = \begin{pmatrix} b_{11} & b_{12} & b_{13} \\ b_{21} & b_{22} & b_{23} \\ b_{31} & b_{32} & b_{33} \end{pmatrix} \tag{5}$$

contributions comprise the unknown coefficients to learn during calibration.

Consider the physics underlying this construction. The permanent dipole moment and resulting magnetic field of the aircraft are static with respect to the coordinate system, with projections onto the total field defined by the direction cosines. From this, it can be seen that $\mathbf{P}$ is the magnetic field vector due to the permanent dipole, with components along the reference frame axes. Note that the numerical indices (1, 2, 3) coincide with the corresponding (x, y, z) axes. The induced

dipole moment can be thought of as resulting from three bars which can be magnetized along the x, y, and z axes, with moments proportional to the earth magnetic field projection onto that axis, but not necessarily located on any axis. In general, each dipole will create a vector field at the origin. This means $\mathbf{A}$ has components a_{ij}, where $u_i a_{ij}$ gives the component of the induced field in the j direction due to the moment pointing in the i direction. A similar argument holds for the geometry and projections of the eddy current fields comprising $\mathbf{B}$. The notable difference is that the eddy currents arise from changes in the magnetic flux through surfaces of the aircraft, which make their contribution proportional to the time derivative of the direction cosines $(\mathbf{u}_t^T)'$. The quadratic form of the second term in Eq. 1 implies that $\mathbf{A}$ can be made symmetric, reducing the number of unknown coefficients for the induced dipole field from 9 to 6, resulting in 18 Tolles-Lawson coefficients. Additional constraints, such as the direction cosine identity $\cos^2 X + \cos^2 Y + \cos^2 Z = 1$ or assumptions about the surfaces of the aircraft, may further reduce the number of terms and coefficients used in the Tolles-Lawson model.

A.2 Learning the Coefficients

Here a linear model is built to determine the unknown Tolles-Lawson coefficients. A row vector of measurements is

$$\boldsymbol{\delta} = \begin{pmatrix} \{u_i\} & \{u_i u_j\} & \{u_i' u_j\} \end{pmatrix} \tag{6}$$

at a given time step, and a matrix of these is measurements is

$$\boldsymbol{\Delta} = \begin{pmatrix} \boldsymbol{\delta}_1 \\ \vdots \\ \boldsymbol{\delta}_{N_t} \end{pmatrix} \tag{7}$$

where each row is one of the N_t timesteps and each column is a term $\cos X$, $\cos Y$, etc. The column vector of coefficients is

$$\boldsymbol{\theta} = \begin{pmatrix} \{p_i\} & \{a_{ij}\} & \{b_{ij}\} \end{pmatrix} \tag{8}$$

Because the magnitude of the total field $H_t = H_{at} + H_{et}$ is the sum of the projections of the aircraft and earth magnetic field onto the total magnetic field, the $N_t \times 1$ column vector $\mathbf{h}_t$ of total field measurements H_t from the scalar magnetometer can be expressed as

$$\mathbf{H} = \boldsymbol{\Delta}\boldsymbol{\theta} + \mathbf{H}_{et} \tag{9}$$

where $\mathbf{h}_{et}$ is the column vector of H_{et} at each timestep, which cannot be measured directly.

To decouple the aircraft field from the earth field, it is helpful to identify a band in which the frequency content of the aircraft dominates the signal. The calibration flight pattern, Figure 3b is roughly a square, with roll, pitch and yaw maneuvers performed along each leg. It can be helpful to think of these maneuvers as injecting aircraft magnetic field content into a given band. The square pattern is repeated in opposite directions, and is flown at high altitude with as tight turns as possible. While the frequency band of interest for magnetic navigation is between 1 mHz and 1 Hz, a band of 0.1 - 0.9 Hz is typically used for calibration. Applying a bandpass filter both sides of Eq. 9 gives

$$\text{bpf}(\mathbf{H}) = \text{bpf}(\boldsymbol{\Delta})\boldsymbol{\theta} + \text{bpf}(\mathbf{H}_{et}). \tag{10}$$

If the bandpass-filtered earth magnetic field projection is zero, i.e. $\text{bpf}(\mathbf{H}_{et}) = 0$,

$$\mathbf{y} = \mathbf{D}\boldsymbol{\theta} \tag{11}$$

where $\mathbf{y} = \text{bpf}(\mathbf{H}_t)$ and $\mathbf{D} = \text{bpf}(\boldsymbol{\Delta})$. Solving for the coefficient vector $\boldsymbol{\theta}$ using linear regression,

$$\boldsymbol{\theta} = (\mathbf{D}^T\mathbf{D})^{-1}\mathbf{D}^T y \tag{12}$$

or ridge regression,

$$\boldsymbol{\theta} = (\mathbf{D}^T\mathbf{D} + \lambda\mathbf{I})^{-1}\mathbf{D}^T y \tag{13}$$

with ridge parameter λ, which is useful as the moment matrix $\mathbf{D}^T\mathbf{D}$ is often poorly conditioned. Learning the Tolles-Lawson coefficients $\boldsymbol{\theta}$ completes the calibration.

Compensation is performed by applying the Tolles-Lawson coefficients to the instantaneous values of the terms derived from vector magnetometer measurements and subtracting this contribution from the magnitude of the total measured field. In symbolic form, the magnitude of the earth's field along the total field is

$$H_{et} = H_t - \boldsymbol{\delta\theta}. \tag{14}$$

The Tolles-Lawson coefficients represent the average contributions of the aircraft magnetic field over the calibration flight. They are determined using band-pass filtered measurements, but applied to unfiltered measurements. There is no directional dependence with respect to the earth's field. See [4] for additional discussion of additive noise, cases where the filtered earth magnetic field signal cannot be ignored, and errors of the vector magnetometer.

Appendix B Datafields

Along with magnetic flux and scalar data, additional fields from sensors on the aircraft are recorded. These fields reflect some of the changes in the aircraft's virtual dipole, causing error in the magnetic scalar sensors, and therefore provide additional de-noising information. Below is a description of each data field.

Table 3: Data Fields

Name	Size	Units	Description
LINE	8	-	Line Number XXXX.YY; XXXX=line and YY=segment
FLT	5	-	Flight Number
YEAR	5	s	Year
DOY	4	m	Day of year
TIME	9	m	* Fiducial Seconds Past Midnight UTC
UTM-X	11	m	X coordinate, WGS-84 UTM ZONE 18N
UTM-Y	11	m	Y coordinate, WGS-84 UTM ZONE 18N
UTM-Z	8	m	Z coordinate, GPS Elevation (above WGS-84 Ellipsoid)
MSL-Z	8	m	Z coordinate, GPS Elevation (above EGM2008 Geoid)
LAT	13	deg	Latitude, WGS-84
LONG	13	deg	Longitude, WGS-84
BARO	8	m	Barometric Altimeter

RADAR	8	m	Filtered Radar Altimeter*
TOPO	8	m	Radar Topography (above WGS-84 Ellipsoid)
DEM	8	m	Digital Elevation Model from SRTM (above WGS-84 Ellipsoid)
DRAPE	8	m	Planned Survey Drape (above WGS-84 Ellipsoid)
PITCH	7	nT	INS computed aircraft pitch
ROLL	7	nT	INS computed aircraft roll
AZIMUTH	7	nT	INS computed aircraft azimuth
DIURNAL	11	nT	Measured Diurnal
COMPMAG1	11	nT	Mag 1: Compensated Airborne Magnetic Field
LAGMAG1	11	nT	Mag 1: Lag Corrected Airborne Magnetic Field
DCMAG1	11	nT	Mag 1: Diurnal Corrected Airborne Magnetic Field
IGRFMAG1	11	nT	Mag 1: IGRF and Diurnal Corrected Airborne Magnetic Field
UNCOMPMAG1	11	nT	Mag 1: Uncompensated Airborne Magnetic Field
UNCOMPMAG2	11	nT	Mag 2: Uncompensated Airborne Magnetic Field
UNCOMPMAG3	11	nT	Mag 3: Uncompensated Airborne Magnetic Field
UNCOMPMAG4	11	nT	Mag 4: Uncompensated Airborne Magnetic Field
UNCOMPMAG5	11	nT	Mag 5: Uncompensated Airborne Magnetic Field
FLUXB_X	11	nT	Flux B: Fluxgate X-axis
FLUXB_Y	11	nT	Flux B: Fluxgate Y-axis
FLUXB_Z	11	nT	Flux B: Fluxgate Z-axis
FLUXB_TOT	11	nT	Flux B: Fluxgate Total
FLUXC_X	11	nT	Flux C: Fluxgate X-axis
FLUXC_Y	11	nT	Flux C: Fluxgate Y-axis
FLUXC_Z	11	nT	Flux C: Fluxgate Z-axis
FLUXC_TOT	11	nT	Flux C: Fluxgate Total
FLUXD_X	11	nT	Flux D: Fluxgate X-axis
FLUXD_Y	11	nT	Flux D: Fluxgate Y-axis
FLUXD_Z	11	nT	Flux D: Fluxgate Z-axis
FLUXD_TOT	11	nT	Flux D: Fluxgate Total
OGS_MAG	11	nT	OGS Survey Diurnal Corrected, Levelled, Mag. Field**
OGS_HGT	8	m	OGS Survey Flown GPH Height (above WGS-84 Ellipsoid)**
INS_ACC_X	12	m/s2	INS X Acceleration
INS_ACC_Y	12	m/s2	INS Y Acceleration
INS_ACC_Z	12	m/s2	INS Z Acceleration
INS_WANDER	12	rad	INS Computed wander angle (ccw from North)
INS_LAT	13	rad	INS Computed Latitude
INS_LON	13	rad	INS Computed Longitude
INS_HGT	8	rad	INS Computed Height (above WGS-84 Ellipsoid)
INS_VEL_N	12	m/s	INS Computed North Velocity
INS_VEL_W	12	m/s	INS Computed West Velocity
INS_VEL_V	12	m/s	INS Computed Vertical Velocity
PITCHRT	10	deg/s	Avionics Computed Pitch Rate
ROLLRT	10	deg/s	Avionics Computed Roll Rate
YAWRT	10	deg/s	Avionics Computed Yaw Rate
LONG_ACC	10	m/s2	Avionics Computed Longitudinal Acceleration
LAT_ACC	10	m/s2	Avionics Computed Lateral Acceleration

NORM_ACC	10	m/s2	Avionics Computed Normal (Vertical) Acceleration
TRUE_AS	10	m/s	Avionics Computed True Airspeed
PITOT_P	10	kPa	Avionics Computed Pitot (Impact) Pressure
STATIC_P	10	kPa	Avionics Computed Static Pressure
TOT_P	10	kPa	Avionics Computed Total Pressure
CUR_COMR	10	A	Current Sensor: COM1 Aircraft Radio
CUR_ACHR	10	A	Current Sensor: Air Conditioner Fan High
CUR_ACLo	10	A	Current Sensor: Air Conditioner Fan Low
CUR_TANK	10	A	Current Sensor: Cabin Fuel Pump
CUR_FLAP	10	A	Current Sensor: Flap Motor
CUR_STRB	10	A	Current Sensor: Strobe Lights
CUR_SRVO_O	10	A	Current Sensor: INS Outer Servo
CUR_SRVO_M	10	A	Current Sensor: INS Middle Servo
CUR_SRVO_R	10	A	Current Sensor: INS Inner Servo
CUR_IHTR	10	A	Current Sensor: INS Heater
CUR_ACPWR	10	A	Current Sensor: Aircraft Power
CUR_OUTPWR	10	A	Current Sensor: System Output Power
CUR_BATR	10	A	Current Sensor: Battery 1
CUR_BAT2	10	A	Current Sensor: Battery 2
V_ACPWR	10	V	Voltage Sensor: Aircraft Power
V_OUTPWR	10	V	Voltage Sensor: System Output Power
V_BATR	10	V	Voltage Sensor: Battery 1
V_BAT2	10	V	Voltage Sensor: Battery 2
V_RESp	10	V	Voltage Sensor: Resolver Board +
V_RESn	10	V	Voltage Sensor: Resolver Board -
V_BACKp	10	V	Voltage Sensor: Backplane +
V_BACKn	10	V	Voltage Sensor: Backplane -
V_GYRO1	10	V	Voltage Sensor: Gyro 1
V_GYRO2	10	V	Voltage Sensor: Gyro 2
V_ACCp	10	V	Voltage Sensor: INS Accelerometers +
V_ACCn	10	V	Voltage Sensor: INS Accelerometers -
V_BLOCK	10	V	Voltage Sensor: Block
V_BACK	10	V	Voltage Sensor: Backplane
V_SERVO	10	V	Voltage Sensor: Servos
V_CABT	10	V	Voltage Sensor: Cabinet
V_FAN	10	V	Voltage Sensor: Cooling Fan

Appendix C Flight Number 1002

The first full flight began with an FOM test at the standard flight location over Shawville, Quebec, at the standard altitude (10,000ft MSL). All sensors were recording en route between Ottawa and FOM area. Then the aircraft flew 3 traverse lines and 2 control lines using drape GPS guidance. The purpose of this was to compare the repeat traverse and control lines to the original map data, and look for measurement agreement to 1-3 nT when the expected map data and actual measurements were compared with their means removed. Additionally, this flight was used to determine

that because there was a trivial difference in accuracy between traverse lines and tie lines, the map is fully sampled.

Starting near the south end of the Eastern traverse line, the aircraft completed free fly portion. This allowed for analysis regarding the amount that upward continuation of drape surface to constant altitude degrades the measurement quality. The pilots caused different magnetic events that were expected to alter the virtual dipole of the aircraft. The table of events is shown in figure 4. Finally, the aircraft continued the free flight while changing altitudes, conducted a final FOM test, and completed the flight.

Table 4: In-flight Events for Flight Number 1002

Time (s)	Messages
46390.87	BOX 1 START
46964.47	BOX 1 END
47027.11	BOX 2 START
47546.27	BOX2 END
49472.03	FUEL PUMP ON
51764.03	FUEL PUMP OFF
52860.64	FUEL PUMP ON
53778.77	FUEL PUMP OFF
56350.25	FUEL PUMP ON
57068.39	FUEL PUMP OFF
57996.02	RADIO TALK
58011.97	RADIO TALK END
58048.73	LIGHTS ON
58186.87	LIGHTS OFF
58229.47	MOVE FERROUS PIPE
58437.77	MOVE FERROUS PIPE
58557.09	ACTION FLAPS
58679.99	END ACTION FLAPS
58964.22	ELECTRIC FAN ON
59225.42	ELECTRIC FAN OFF
59244.63	AIR CON FANS HIGH
59543.09	VARY SPEED
59791.94	END SPEED VARIATION
59852.06	AIRCRAFT ELECTRICS VARY
59959.14	AIRCRAFT ELECTRICS SURVEY CONFIG
61954.49	RADIO MIC START
61999.92	RADIO MIC END
62035.57	LIGHT ON
62171.23	LIGHTS OFF
62184.84	MOVE FERROUS PIPE
62370.84	FERROUS PIPE STOWED
62395.09	MOVE FLAPS
62548.82	END MOVE FLAPS

62566.68	ELECTRIC FAN ON
62737.01	ELECTRIC FAN OFF
62759.29	VARY PEED START
62978.37	END VARY SPEED
64309.45	RADIO MIC START
64357.46	RADIO MIC END
64430.01	LIGHTS ON
64580.20	LIGHTS OFF
64637.38	MOVE FERROUS PIPE
64819.54	STOW FERROUS PIPE
64890.42	MOVE FLAPS
65017.70	END MOVE FLAPS
65058.05	ELECTRIC FAN ON
65277.54	ELECTRIC FAN OFF
65303.63	VARY SPEED
65471.15	END VARY SPEED
65540.91	WEATHER RADAR ON
65696.36	WEATHER RADAR OFF
66571.73	BOX 1 START
67131.80	BOX 1 END
67276.84	BOX 2 START
67839.15	BOX 2 END

Appendix D Flight Number 1004

Flight Number 1004 occurred over the Eastern free flight area at 800m HAE. The line spacing was less than the height above ground level, and the flight covered as much area as possible (∼40x10 km). The purpose of this pattern was to create a high resolution survey area for future flights. For flight events see table 5.

Table 5: In-flight Events for Flight Number 1004

Time (s)	Message
45555.4856	Cabin fuel pump on
48693.3937	Cabin fuel pump off
49207.2425	Pilot went to back
50141.8761	Cabin fuel pump on
51632.9739	Cabin fuel pumps off
53624.2481	Cabin tank pump on
54224.0937	Cabin tank pump off
56066.4593	Autopilot on
56346.8474	Autopilot off

Appendix E Flight Number 1005

The aircraft first flew 3 compensation profiles at progressively higher altitudes while varying the state: one at 400m HAE above Eastern survey, and the other two at the normal compensation area at 18,000 ft MSL and standard altitude. For 1 hour, the aircraft followed boxy figure 8's in a high resolution survey area (800m HAE) created on Flight Number 1004. The remaining time consisted of two large flight paths through the Renfrew and Eastern surveys at 400m HAE. For flight events see table 5.

Table 6: In-flight Events for Flight Number 1005

Time (s)	Message
48102.5663	Flaps for vis
50424.5290	Flap up
51154.7356	Flaps
51953.0330	Flaps up
52713.4060	Flaps down
53427.4995	Flaps up
54202.9712	Flaps 10
54967.1475	Flaps up

Appendix F Events for Flight Number 1003

The full list of events for Flight Number 1003 is shown in table 7.

Table 7: In-flight Events for Flight Number 1003

Time (s)	Message
50255.97	WX RADAR ON/OFF
50771.63	IN BOX AREA
51478.22	RADIO 4 MIN AGO. CALL ON COMM 1, COM 2
52313.19	LIGHTS BLINKING
52473.55	LIGHTS BLINKING DONE
52502.45	FUEL PUMPS ON
52710.15	FLAPS 10 SET
52789.00	FLAPS UP
52801.90	FLAPS 10 SET
52845.30	FLAPS UP
52855.62	SLOW SPEED
52886.29	FLAPS 10 SET
52972.02	CRUISE SPEED SET FLAPS UP
53162.23	AC OFF
53183.72	AC VENTILATE
53221.88	AC ON

53247.12	AC OFF
53276.13	AC VENTILATE
53314.81	AC COOL
53327.47	VENT FANS LOW
53415.09	VENT FANS HIGH
53571.45	SLOW FLYING FLAPS 10 SET
53617.75	POWER LINES -20 SECS
53694.19	FAST CRUISE SET FLAPS UP
53740.61	RADAR ON
53833.48	RDAR OFF
53859.12	FUEL PUMPS OFF
53904.28	FUEL PUMPS BOTH ON
53964.02	FUEL PUMP OFF
53983.30	RADAR ON
54029.08	FUEL PUMPS ON
54059.43	RADAR OFF
54134.80	CABIN FUEL PUMP 2 OFF 1 ON
54156.64	RADIO CALL
54191.02	SATPHONE CALL
54316.52	SATPHONE CALL COMPLETE
54537.99	CLIMB TO 800M
54644.55	ESTABLISHED AT 800M
54720.53	VISUAL BELOW CLOUD BELOW DRAPE
54940.59	BLINKING LIGHTS
55087.75	SURVEY CONFIG
55097.88	RADAR ON
55194.06	RADAR OFF
55345.18	AC OFF VENT FANS LOW
55414.64	AC VENTILATE FANS LOW
55554.88	AC COOL VENTS HIGH
55853.15	FLAPS 10
55868.44	FLAPS UP
56171.95	WX RADAR ON
56193.34	SLOW SPEED
56206.55	LAP 10
56263.06	FLAPS UP
56267.19	FASTER
56315.76	WX RADAR STBY
56400.99	CLOUDS
56491.02	RADIO
56520.08	ADF OFF
56712.12	ADF NO
56718.28	CABIN PUMP OFF
56761.12	RADIO COM 1
56775.56	RADIO COM 2
57408.48	RADIO COM 1

57516.18	FALP 10
57549.92	FLAP UP
58155.52	IPAD REBOOT
58223.49	PUUMP 1 ON
58524.69	RADIO COM 2
59023.14	POWEER LINE
59276.62	AUTOPILOT ON A AND OFF
59320.68	WX RADAR STBY
60181.32	OUTSIDE LOOP OF RENFREW AREA
60284.52	CABBIN PUMP OFF. AUX ANK EMPTY
60697.28	LAFP 10
60722.92	FLAP UIUUP
60875.25	RADIO COM 1
61088.71	WX RAR ON
61346.67	CABIN FAN ON
61409.82	CABIN FAN OFF
61486.28	POWER LINES
61753.18	AC OFF VENT FANS LOW
61796.00	AIR CONDITIONING VENTILATE, VENT FANS LOW
61855.22	AIR CON ON VENT FANS LOW
61889.22	SLOW FLYING FLAPS 10
62023.35	NORMAL CRUISE SPEED, FLAPS UP
62046.87	AIR CON COOL VENT FANS HIGH
62279.05	LIGHTS ON (TROBE NAV BEACON)
62444.25	LIGHTS OFF((STROBE NAV BKN), PULSE ON
62555.24	RADAR ON
62618.49	RADAR STANDBY
63058.44	RADIO CALL
63512.03	RADIO CALL
64085.56	SLOW FLYING FLAPS 10 SET
64174.04	FLAPS UP NORMAL CRUISE
64672.43	STARTING RENFREW800M
64854.07	AIR CON OFF VENT FANS HIGH
64945.69	AIR CONT TO VENTILATE VENT FANS HIGH
65024.72	AIR CON COOL VENT FANS HIGH
65334.50	WX RADAR ON
65386.44	WX RADAR STBY
65945.85	RADIO COM 1
66034.53	WX RADR ON
66057.69	WX RADAR STBY
66319.00	CABIN FAN ONO
66473.86	CABIN FAN OFF
66899.37	WX RADAR ON
67401.28	WX RADAR ON
67455.51	WX RADAR STBY
67909.38	FLAPS 10

67915.84	SLOWING TO 100KTS
67992.56	FLAPS UP
68000.05	SPEEDING UP BACK TO NORMAL CRUISE
68320.24	WX RADR ON
68335.98	WX RADR STBY

Acknowledgements

The authors appreciate support from the MIT-Air Force Artificial Intelligence Accelerator, a joint collaboration between the Air Force, MIT CSAIL, and Lincoln Laboratory.

References

[1] Walter E. Tolles. Magnetic field compensation system, April 1955. US Patent 2,706,801.

[2] Sander Geophysics Ltd. High resolution magnetic gradiometer surveys, 2020.

[3] Aaron J. Canciani. *Absolute Positioning Using the Earth's Magnetic Anomaly Field*. PhD thesis, Air Force Institute of Technology, 2016.

[4] Q. Han, Z. Dou, X. Tong, X. Peng, and H. Guo. A modified tolles–lawson model robust to the errors of the three-axis strapdown magnetometer. *IEEE Geoscience and Remote Sensing Letters*, 14(3):334–338, 2017.